Well-Aligned Cone-Shaped Nanostructure of Polypyrrole/RuO2 and Its Electrochemical Supercapacitor

ARTICLE *in* THE JOURNAL OF PHYSICAL CHEMISTRY C · AUGUST 2008

Impact Factor: 4.77 · DOI: 10.1021/jp8049558

9 AUTHORS, INCLUDING:

Chang Li
Xin Xiang Medical University
392 PUBLICATIONS **13,150** CITATIONS
SEE PROFILE

Xiaoqiang Cui
Jilin University
67 PUBLICATIONS **1,793** CITATIONS
SEE PROFILE

Chang Qing Sun
Nanyang Technological University
385 PUBLICATIONS **6,092** CITATIONS
SEE PROFILE

Keryn Lian
University of Toronto
88 PUBLICATIONS **870** CITATIONS
SEE PROFILE

Well-Aligned Cone-Shaped Nanostructure of Polypyrrole/RuO_2 and Its Electrochemical Supercapacitor

Jianfeng Zang,[†,‡] Shu-Juan Bao,[†] Chang Ming Li,[*,†] Haijiao Bian,[‡] Xiaoqiang Cui,[†] Qiaoliang Bao,[†] Chang Q. Sun,[‡] Jun Guo,[§] and Keryn Lian[||]

School of Chemical and Biomedical Engineering and Center for Advanced Bionanosystems, Nanyang Technological University, 70 Nanyang Drive, Singapore 637457, School of Electrical & Electronic Engineering, Nanyang Technological University, 50 Nanyang Avenue, Singapore 639798, School of Materials Science and Engineering, Nanyang Technological University, Nanyang Avenue, Singapore 639798, and Department of Materials Science and Engineering, University of Toronto, Toronto, Ontario, Canada

Received: June 5, 2008; Revised Manuscript Received: July 15, 2008

A new well-aligned cone-shaped nanostructure of polypyrrole (WACNP) has been successfully grown on Au substrate by using a simple, one-step, reliable, and template-free anodic deposition method. The formation mechanism of WACNP is proposed, in which the hydrogen bonding introduced from phosphate buffer solution (PBS) promotes the formation of a well-aligned nanostructure of polypyrrole (PPy), while the steric hindrance effect arisen from high concentration of pyrrole (Py) boosts its vertical alignment and further forms a cone-shaped nanostructure. The 3D, arrayed, nanotubular architecture coated with an ultrathin layer of RuO_2 by the magnetron sputtering deposition method was tailored to construct a supercapacitor. The unique structure and design not only reduces the diffusion resistance of electrolytes in the electrode material but also enhances its electrochemical performance. The modification of RuO_2 on WACNP results in a capacitance higher than that of WACNP by three times. The specific capacitance of RuO_2/WACNP is 15.1 mF cm^{-2} ($\sim$302 F g^{-1}) measured by the charge−discharge method with an applied current density of 0.5 mA cm^{-2} over a potential range of −0.2 to 0.7 V, and is greater than that of commercial carbon materials by 2−3 orders of magnitude. The high capacitance and good stability of the RuO_2/WACNP electrode is very promising for applications in microsupercapacitor devices.

Introduction

Nanomaterials with the hierarchical design of well-defined and highly oriented 3-dimensional (3D) arrays consisting of 1-dimensional (1D) nanostructures such as carbon nanotubes and nanowires of semiconductors, metals, and oxides have been under intense investigation recently.[1−3] The 3D arrays demonstrate unique properties and advantages over randomly oriented 1D nanostructures in various applications such as chemical/biological sensing, electron emission, energy conversion and storage, microelectronics, and catalysis.[4,5] However, there was little success in alignment of 1D nanostructures of conductive polymer on a large area until the pioneer work was done by Martin, who used mesoporous templates to grow the aligned polypyrrole (PPy).[6] However, the approach uses a strong acidic or basic medium to dissolve the membranes, which not only damages the products but also brings out safety concerns and environmental hazards. Recently some methods such as nanoimprint and direct laser interference micro/nanopatterning[7,8] have been developed to produce conductive polymeric arrays. These methods involve either hash conditions or complicated technologies, and thus suffer from environmental contaminations, limited substrate selection, or high cost. A practical route to manufacture thin film devices on complicated physical areas on a large scale and at an affordable cost still requires great ingenuity. Thus, we are reporting here a unique and simple template-free, low-temperature electrodeposition approach to fabricate large orientally nanostructured conductive polymer arrays in an aqueous solution. The electrochemical deposition can be used to easily tailor 1D nanostructure on complicated surfaces (such as on a microelectrode surface) by simply varying current or potential, which is particularly essential in fabrications of microdevices for various applications.

PPy has been intensively studied as a potential energy storage material because of its intrinsic electrical conductivity, redox properties, and relatively low cost.[9−13] Electrochemical capacitors (EC) are often used as energy storage systems for high power supply. It is very critical for a capacitor to have high energy density and high power density for practical power source applications. High energy and high power density of an electrochemical capacitor require high specific capacitance and low specific internal resistance, respectively, of which the energy density can be enhanced by high specific surface area, wide potential window, and multiple electrochemical redox reactions of electrode materials, while the power density can be improved by high conductivity and low Faraday resistance of the electrodes. One strategy to improve the EC performance is to "activate" the conductive polymers by columnar morphology, ion doping, redox species immobilization, and enhancement of polymer conjugation and orientation.[14−17] Polymer nanocomposites that can possess unique hybrid properties of neither the incorporated components nor the host matrices have been studied

* Corresponding author: C. M. Li, E-mail: ecmli@ntu.edu.sg; Tel: +65-67904485; Fax: +65-67911761.
† School of Chemical and Biomedical Engineering and Center for Advanced Bionanosystems, Nanyang Technological University.
‡ School of Electrical & Electronic Engineering, Nanyang Technological University.
§ School of Materials Science and Engineering, Nanyang Technological University.
|| Department of Materials Science and Engineering, University of Toronto.

10.1021/jp8049558 CCC: $40.75
Published on Web 08/28/2008

in recent years.[11,18−20] This approach is also used to incorporate high specific capacitance materials like carbon nanotubes, metal oxide into a conductive polymer for significant improvement of the supercapacitance.[21−25] Among all these composed materials, hydrous ruthenium oxide is recognized as the best supercapacitor material because of its extremely high specific capacitance, highly reversible redox reactions, wide potential window, superior conductivity, and excellent cycleability.[26−28] However, its high specific capacitance is hindered by electrode kinetic limitation, which causes the very outside surface thin layer of RuO_2 to participate in the charge-storage process while the rest of the material remains inactive.[29−31] It is reported that a 3D mesoporous structure with ordered array architecture can significantly reduce the diffusion resistance of reactant.[32−35] To not only reduce the electrode kinetic limitations such as Faraday and diffusion resistance but also efficiently utilize RuO_2, a 3D mesoporous structured conductive polymer/RuO_2 composite with ordered array architecture may overcome the kinetic limitation in the porous electrode.

In this work, we developed a simple, one-step, and template-free approach to grow on a large-scale a well-aligned cone-shaped nanostructure of PPy (WACNP). Such an ordered PPy nanostructure has not been reported yet. On the basis of the experimental results, a formation mechanism of the WACNP structure is proposed. Furthermore, the magnetron sputtering method is used to deposit an ultrathin layer of RuO_2 on the polymer surface with the 3D arrayed architecture. The combination of high surface area of the unique structure of PPy with the high specific capacitance RuO_2 was tailored to construct a supercapacitor, of which the electrochemical properties were systematically studied and compared with the WACNP-based capacitors.

Experimental Methods

All chemicals were purchased from Aldrich and were of analytical grade except as indicated. Pyrrole (Py) was distilled under reduced pressure. Phosphate buffer solutions (PBSs) with pH 6.8 were prepared with deionized (DI) water by adjusting the molar ratio of $[Na_2HPO_4]/[NaH_2PO_4]$.

WACNP was potentiostatically electropolymerized at 0.85 V vs Ag/AgCl in an aqueous solution containing 0.6 M Py and 0.2 M PBS, pH 6.8. A 300 nm gold film deposited on a silicon wafer with an intermediate layer of Ti was used as the working electrode. The as-prepared WACNP and a bare gold film were placed in a sputtering chamber to coat RuO_2 by magnetron sputtering deposition with a 3-in. ruthenium target at a power of 220 W for 5 min in an Ar/O_2 atmosphere.[36] The flow rate of Ar and O_2 was 10 and 30 sccm (sccm denotes cubic centimeter per minute at STP), respectively. In the procedure, the sputtered Ru was oxidized in oxygen and deposited on the PPy.

The morphologies of the PPy products were investigated with JSM-6700F FESEM (Japan) and HRTEM (JEM-2100F, Japan). The X-ray diffraction (XRD) pattern was obtained with an XRD instrument (Bruker AXS X-ray diffractionmeter, Germany). The electrochemical synthesis and measurements were performed in a three-electrode cell, using a CHI-660B electrochemical station (CH Instruments Inc. USA). The electrochemical measurements were performed in 1 M H_2SO_4 with a platinum sheet and Ag/AgCl as the counter and reference electrode, respectively.

Results and Discussion

WACNP was grown on Au substrate on a large scale by a template-free electrochemical method. The FESEM images in Figure 1 clearly show that the produced PPy has a tubular, cone-shaped nanostructure with vertical orientation on the substrate. The outer and inner diameters of the PPy nanocone tip are 66 ± 26 and 20 ± 10 nm, respectively. The apex angle of the PPy nanocone is $22 \pm 5°$, which provides a higher mechanical and thermal stability than a narrow tube or cylinder. The space between the tips of nanocones is spacious and much larger than the outer diameter of the cone, which is very convenient for further modification and electrochemical accessibility.

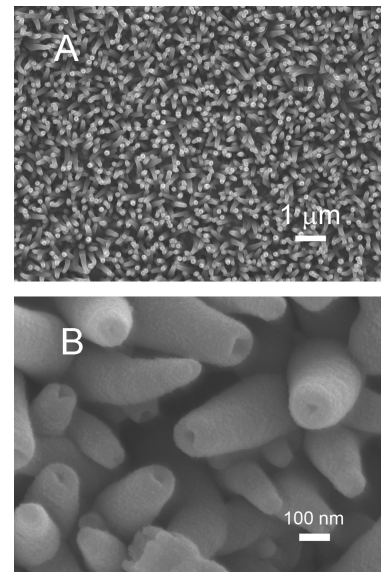

Figure 1. FESEM images of the well-aligned cone-shaped nanostructure of PPy at low magnification (A) and high magnification (B).

In our previous work, PPy nanofiber was template-free synthesized in an aqueous solution. The nanofiber formation is driven by the hydrogen bonding between the N−H group of the Py ring and the oxygen atom of the phosphate anions, while being blocked by the electrostatic interactions between the positively charged Py oligomers and dopant ClO_4^-.[37] In this work, when polymerization was conducted with a solution containing zero $[ClO_4^-]$ and a high concentration of Py, a new vertically well-aligned cone-shaped nanostructure of PPy was formed as shown in Figure 1, which is different from the 1D nanostructured PPy prepared in our previous work. As discussed in our previous work, the presence of PBS in the monomer solution only promotes formation of the 1D nanostructured PPy. The vertical alignment of the PPy cone nanostructure is most likely ascribed to the high concentration of Py, which causes a steric hindrance effect as shown in Scheme 1. This is a model widely accepted to interpret the vertically growth aligned carbon nanotube.[38,39] In more detail, when Py reaches a certain high concentration, the density of nucleation sites on the substrate is greatly increased (Scheme 1, step A), resulting in prohibited growth of PPy nanostructure in directions other than vertical direction due to the steric hindrance from the adjacent PPy (Sch 1, steps B and C). Apparently, the steric hindrance effect is getting stronger and stronger with the PPy growth progress. This can lead to the formation of cone-shaped product with larger diameter at its bottom and smaller diameter at its tip.

The mechanism here is supported by the result of low- angle XRD of WACNP, which shows an intense peak centered at $2\theta = 4.84°$ (Figure 2A). The corresponding Bragg spacing $d = 1.83$ nm is assigned as the periodic distance of the aligned PPy chains, indicating the existence of short-range-ordered bundles in the product.[40−42] The result is consistent with our previous XRD result of PPy nanofiber prepared in the presence of both PBS and ClO_4^-.

SCHEME 1: Schematic Drawing of the Growth of WACNP[a]

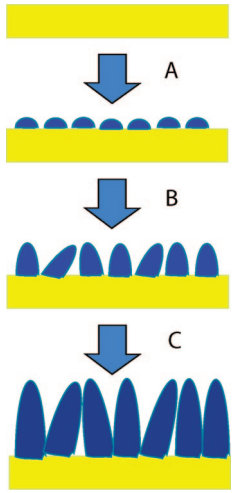

[a] A: High density of nucleation sites. B: Initial alignment of PPy due to steric hindrance effect. C: Vertical alignment of PPy in the following growth.

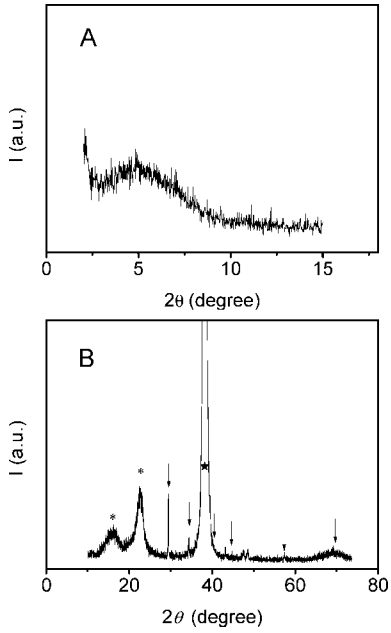

Figure 2. XRD patterns for (A) WACNP and (B) RuO_2/WACNP.

The prepared WACNP was further modified with a thin layer of RuO_2 by magnetron sputtering of metallic Ru in an atmosphere of O_2 and Ar (3:1). The crystal structure of RuO_2-coated WACNP was characterized by XRD, as shown in Figure 2B. The XRD pattern shows reflections of PPy, RuO_2, and Au substrate. The two peaks at $2\theta = 16.2°$ and 22.8° are assigned to PPy.[43] The strongest peak at $2\theta = 38.1°$ is from Au substrate (ICSD No. 89-3697). The peaks indicated by arrows are from RuO_2 (ICSD No. 73-1469). No reflections for Ru metal or metal carbides are observed, clearly indicating that the RuO_2 was successfully coated onto the WACNP during the sputtering deposition.

TEM was carried out for a more detailed structure. The sample was prepared by sonication for 1 h in DI water followed by its deposition on a TEM copper grid. Figure 3A presents an overview of an individual PPy nanocone, clearly showing that the cone-shaped PPy nanostructure was coated with an ultrathin layer of RuO_2. Near the tip, the coating layer is thicker, about

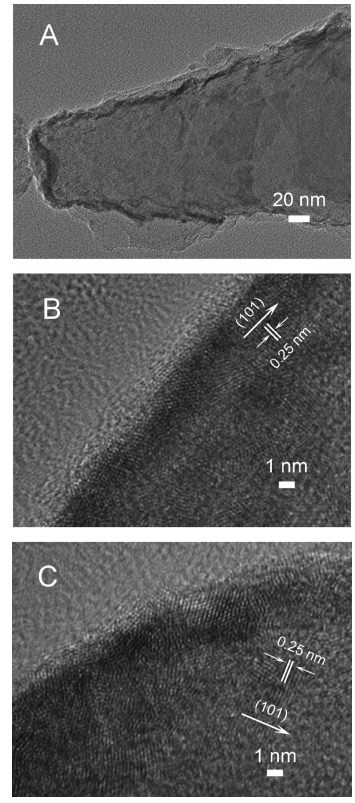

Figure 3. (A) TEM image of a typical PPy nanocone coated with RuO_2; (B) HRTEM image of the crystalline RuO_2 coated on the sidewall of the PPy nanocone; (C) HRTEM image of the crystalline RuO_2 coated on the tip of the PPy nanocone.

10 nm in thickness. The layer of RuO_2 at the sidewall is about 5 nm in thickness, thinner than that at the tip, which is possibly caused by partial shielding from the tips of the neighboring cones. In the high-resolution TEM (HRTEM) images taken from the sidewall (Figure 3B) and the tip (Figure 3C) of the nanocone, the lattice fringes are clearly visible with a spacing of 0.25 nm, which is in good agreement with the spacing of the (101) plane of the crystal RuO_2. The TEM result is consistent with the above XRD result, and confirms that an ultrathin layer of single-crystalline RuO_2 is successfully coated on the WACNP. From TEM images, we can also conclude that the adhesion of RuO_2 on the walls of the cone is very strong even though the sample was sonicated for 1 h during the TEM sample preparation process.

Both prepared WACNP and RuO_2/WACNP were used to make supercapacitor electrodes and were characterized by using cyclic voltammetry (CV) and electrochemical impedance spectroscopy (EIS) measurements. The representative CV curves measured with these electrodes in 1 M H_2SO_4 are presented in Figure 4, which show a capacitance characteristic, a rectangular shape, but distinguished from that of electric double-layer capacitance. One pair of defined redox peaks are clearly visible in both CV curves, implying that the measured capacitance is mainly contributed from the pseudocapacitance caused by reversible electrochemical reactions. Comparing curves A and B of Figure 4, the CV curve enclosed area for the RuO_2/WACNP is about four times as large as that of the WACNP, demonstrating a much larger capacitance from the RuO_2/WACNP. Obviously, the significant capacitance should come from the thin layer of RuO_2. The CV curve-enclosed area of RuO_2/WACNP is also significantly larger than that of the RuO_2-coated bare gold film (data not shown here), because the array

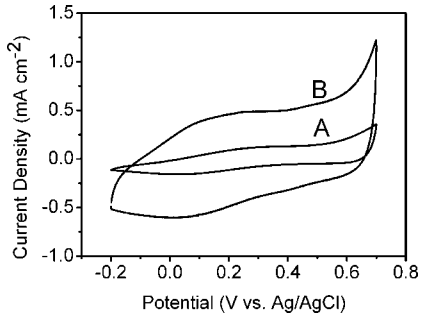

Figure 4. CVs of the bare WACNP electrode (A) and the RuO_2/WACNP electrode (B) in 1 M H_2SO_4 at a scan rate of 20 mV s^{-1}.

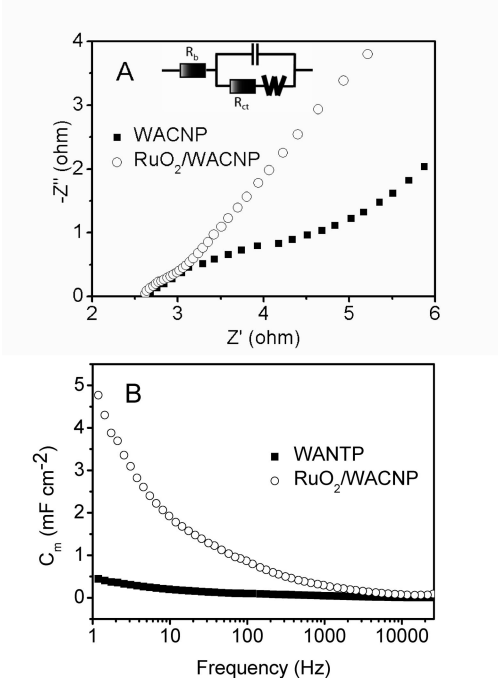

Figure 5. AC impedance spectra of the bare WACNP electrode (solid square) and the RuO_2/WACNP nanocomposite electrode (empty circle): (A) Nyquist plots at ac voltage amplitude of 5 mV; (B) Bode plots from impedance spectroscopic analysis.

architecture introduces a high specific surface area. This is very significant for its practical application. Although RuO_2 is a superior pseudocapacitance material, the relatively high cost of the material limits its practical applications. Apparently, the ultrathin coating of RuO_2 can provide full utilization efficiency while greatly reducing the cost for its capacitor applications.[29−31]

Figure 5A shows the Nyquist plots with well-defined semicircles over the high-frequency range, followed by a straight sloped line in the low-frequency region measured from both WACNP and RuO_2/WACNP. The diameter of the semicircle corresponds to the interfacial charge-transfer resistance (R_{ct}), which is called the Faraday resistance and is often the limiting factor for the power density of a pseudocapacitor.[44] The EIS pattern can be fitted by an equivalent circuit as shown in the inset of Figure 5A and the calculated R_{ct} of RuO_2/WACNP is 0.2 ohm, which is much smaller than the 3.1 ohm of WACNP. Such a low Faraday resistance could significantly boost the power density produced by the pseudocapacitance. The Bode plots of the two electrodes for the specific capacitance are presented in Figure 5B. For frequencies from 1 to ~1000 Hz, the specific capacitance of the RuO_2/WACNP electrode is significantly higher than that of the bare WACNP electrode. Further, since the RuO_2/WACNP electrode has very low

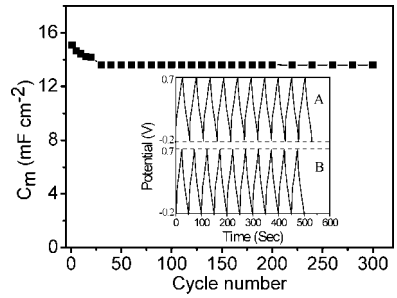

Figure 6. The cyclic life of the RuO_2/WACNP electrode during charge−discharge with an applied current density of 0.5 mA cm^{-2} in 1 M H_2SO_4 between −0.2 and +0.7 V. The insets are its first ten cycles (A) and the last ten cycles (B) of the charge−discharge curve.

impedance over a broad frequency range, it could provide various applications over a wide frequency range.

Charge−discharge performance measurements were focused on the RuO_2/WACNP electrode as shown in the insect of Figure 6. During the charge and discharge steps, the curves display two variation ranges. A perfect variation of potential vs time (−0.2 to 0.2V) parallel to the potential axis indicates a pure double-layer capacitance behavior from the charge separation at the electrode/electrolyte interface, and a sloped variation of the potential vs time (0.2 to 0.7 V) shows a typical pseudocapacitance behavior, caused by the electrochemical redox reaction at the electrode/electrolyte interface.[45] The symmetry of the charge and discharge characteristic indicates that the RuO_2/WACNP has excellent capacitance characteristics and a superior reversible redox reaction. The specific capacitance of the electrode at different current density is calculated by $C_m = j \times \Delta t/\Delta V$ from the discharge curves, where j is the constant discharge current density, Δt is the discharge time, and ΔV is the potential drop during discharge. The specific capacitance value is 15.1 mF cm^{-2} (~302 F g^{-1}) for the RuO_2/WACNP electrode with an applied current density of 0.5 mA cm^{-2} in the potential range of −0.2 to 0.7 V, which is a two to three orders of magnitude increase compared to commercial carbon materials reported in the literature.[46] The electrochemical performance is also competitive compared with the nanocomposite of carbon nanotube/conducting polymer and carbon nanotube/RuO_2.[36,47]

The electrochemical stability of the RuO_2/WACNP electrode in 1 M H_2SO_4 electrolyte was examined by chronopotentiometry at 0.5 mA cm^{-2} in the potential range of −0.2 to 0.7 V. Figure 6 shows the specific capacitance of the RuO_2/WACNP electrode based supercapacitor with respect to the charge−discharge cycle number. The specific capacitance of the nanocomposite electrode declined slightly during the first 30 cycles but remained constant thereafter (constant specific capacitance 13.6 mF cm^{-2}). The specific capacitance can still be 90.0% after 300 charge/discharge cycles. As shown in insets A and B of Figure 6, the curve shape of the last 10 cycles (291−300 cycles) is similar to that of the first 10 cycles. The long-term stability combined with the excellent array architecture and good conductivity make this a promising array for fabricating microsupercapacitor devices.

Conclusions

A well-aligned cone-shaped nanostructure of PPy was successfully grown on Au substrate by using a simple, one-step, cost-effective, template-free, and anodic deposition method. A mechanism for the WACNP formation in an aqueous solution without assistance of any template is proposed, in which the

presence of the hydrogen bonding between phosphate and Py oligomers is essential to produce well-aligned nanostructure, while the steric hindrance effect produced from the high concentration of Py boosts its further vertical alignment. Furthermore, the 3D, arrayed, nanotubular architecture coated with an ultrathin layer of RuO_2 was tailored to construct a supercapacitor. The unique structure and design not only reduces the diffusion resistance of electrolytes in the electrode material but also enhances its electrochemical activity. The specific capacitance and conductivity of RuO_2/WACNP by the modification with an ultrathin layer of RuO_2 was significantly improved in comparison to that of the bare WACNP, which was verified by CVs and EIS for the two electrodes. The good stability of the RuO_2/WACNP electrode is very promising for applications in microsupercapacitor devices.

References and Notes

(1) Li, Y. G.; Tan, B.; Wu, Y. Y. *J. Am. Chem. Soc.* **2006**, *128*, 14258.

(2) Vayssieres, L.; Rabenberg, L.; Manthiram, A. *Nano Lett.* **2002**, *2*, 1393.

(3) Wang, X. D.; Song, J. H.; Li, P.; Ryou, J. H.; Dupuis, R. D.; Summers, C. J.; Wang, Z. L. *J. Am. Chem. Soc.* **2005**, *127*, 7920.

(4) Liu, J.; Lin, Y. H.; Liang, L.; Voigt, J. A.; Huber, D. L.; Tian, Z. R.; Coker, E.; McKenzie, B.; McDermott, M. J. *Chem. Eur. J.* **2003**, *9*, 605.

(5) Kim, B. H.; Park, D. H.; Joo, J.; Yu, S. G.; Lee, S. H. *Synth. Met.* **2005**, *150*, 279.

(6) Martin, C. R. *Science* **1994**, *266*, 1961.

(7) Dong, B.; Lu, N.; Zelsmann, M.; Kehagias, N.; Fuchs, H.; Torres, C. M. S.; Chi, L. F. *Adv. Funct. Mater.* **2006**, *16*, 1937.

(8) Acevedo, D. A.; Lasagni, A. F.; Barbero, C. A.; Mucklich, F. *Adv. Mater.* **2007**, *19*, 1272.

(9) MacDiarmid, A. G. *Angew. Chem., Int. Ed.* **2001**, *40*, 2581.

(10) Li, C. M.; Sun, C. Q.; Chen, W.; Pan, L. *Surf. Coat. Technol.* **2005**, *198*, 474.

(11) Cui, X. Q.; Li, C. M.; Zang, J. F.; Zhou, Q.; Gan, Y.; Bao, H. F.; Guo, J.; Lee, V. S.; Moochhala, S. M. *J. Phys. Chem. C* **2007**, *111*, 2025.

(12) Zhou, Q.; Li, C. M.; Li, J.; Cui, X. Q.; Gervasio, D. *J. Phys. Chem. C* **2007**, *111*, 11216.

(13) Qiao, Y.; Li, C. M.; Bao, S. J.; Bao, Q. L. *J. Power Sources* **2007**, *170*, 79.

(14) Naoi, K.; Oura, Y.; Maeda, M.; Nakamura, S. *J. Electrochem. Soc.* **1995**, *142*, 417.

(15) He, B. L.; Zhou, Y. K.; Zhou, W. J.; Dong, B.; Li, H. L. *Mater. Sci. Eng., A* **2004**, *374*, 322.

(16) Ingram, M. D.; Staesche, H.; Ryder, K. S. *J. Power Sources* **2004**, *129*, 107.

(17) Sharma, R. K.; Rastogi, A. C.; Desu, S. B. *Electrochem. Commun.* **2008**, *10*, 268.

(18) Qiao, Y.; Bao, S. J.; Li, C. M.; Cui, X. Q.; Lu, Z. S.; Guo, J. *ACS Nano* **2008**, *2*, 113.

(19) Cui, X. Q.; Li, C. M.; Zang, J. F.; Yu, S. C. *Biosens. Bioelectron.* **2007**, *22*, 3288.

(20) Xiao, Y. H.; Li, C. M. *Electroanalysis* **2008**, *20*, 648.

(21) Hughes, M.; Chen, G. Z.; Shaffer, M. S. P.; Fray, D. J.; Windle, A. H. *Chem. Mater.* **2002**, *14*, 1610.

(22) Zhou, Y. K.; He, B. L.; Zhou, W. J.; Li, H. L. *J. Electrochem. Soc.* **2004**, *151*, A1052.

(23) Hong, J. I.; Yeo, I. H.; Paik, W. K. *J. Electrochem. Soc.* **2001**, *148*, A156.

(24) Song, R. Y.; Park, J. H.; Sivakkumar, S. R.; Kim, S. H.; Ko, J. M.; Park, D. Y.; Jo, S. M.; Kim, D. Y. *J. Power Sources* **2007**, *166*, 297.

(25) Zhang, X.; Ji, L. Y.; Zhang, S. C.; Yang, W. S. *J. Power Sources* **2007**, *173*, 1017.

(26) Zheng, J. P.; Jow, T. R. *J. Electrochem. Soc.* **1995**, *142*, L6.

(27) Zheng, J. P.; Cygan, P. J.; Jow, T. R. *J. Electrochem. Soc.* **1995**, *142*, 2699.

(28) Chang, K. H.; Hu, C. C. *Electrochem. Solid State Lett.* **2004**, *7*, A466.

(29) Trasatti, S. *Electrochim. Acta* **1991**, *36*, 225.

(30) Liu, T.; Pell, W. G.; Conway, B. E. *Electrochim. Acta* **1997**, *42*, 3541.

(31) Ardizzone, S.; Fregonara, G.; Trasatti, S. *Electrochim. Acta* **1990**, *35*, 263.

(32) Miller, J. M.; Dunn, B.; Tran, T. D.; Pekala, R. W. *J. Electrochem. Soc.* **1997**, *144*, L309.

(33) Che, G. L.; Lakshmi, B. B.; Fisher, E. R.; Martin, C. R. *Nature* **1998**, *393*, 346.

(34) Guo, Y. G.; Hu, Y. S.; Sigle, W.; Maier, J. *Adv. Mater.* **2007**, *19*, 2087.

(35) Hu, C. C.; Chang, K. H.; Lin, M. C.; Wu, Y. T. *Nano Lett.* **2006**, *6*, 2690.

(36) Ye, J. S.; Cui, H. F.; Liu, X.; Lim, T. M.; Zhang, W. D.; Sheu, F. S. *Small* **2005**, *1*, 560.

(37) Zang, J. F.; Li, C. M.; Bao, S. J.; Cui, X. Q.; Bao, Q. L.; Sun, C. Q. Template-free Electrochemical Synthesis of Superhydrophilic Polypyrrole Nanofiber Network, Macromolecules, in press.

(38) Lee, C. J.; Kim, D. W.; Lee, T. J.; Choi, Y. C.; Park, Y. S.; Lee, Y. H.; Choi, W. B.; Lee, N. S.; Park, G. S.; Kim, J. M. *Chem. Phys. Lett.* **1999**, *312*, 461.

(39) Bao, Q. L.; Pan, C. X. *Nanotechnology* **2006**, *17*, 1016.

(40) Cai, Z. H.; Lei, J. T.; Liang, W. B.; Menon, V.; Martin, C. R. *Chem. Mater.* **1991**, *3*, 960.

(41) Zhang, L. J.; Long, Y. Z.; Chen, Z. J.; Wan, M. X. *Adv. Funct. Mater.* **2004**, *14*, 693.

(42) Zhang, L. J.; Wan, M. X. *Adv. Funct. Mater.* **2003**, *13*, 815.

(43) Cheah, K.; Forsyth, M.; Truong, V. T. *Synth. Met.* **1998**, *94*, 215.

(44) Bard, A. J.; Faulkner, L. R. *Electrochemical Methods: Fundamentals and Applications*, 2nd ed.; Wiley: New York, 2001.

(45) Sugimoto, W.; Iwata, H.; Yasunaga, Y.; Murakami, Y.; Takasu, Y. *Angew. Chem., Int. Ed.* **2003**, *42*, 4092.

(46) Frackowiak, E.; Beguin, F. *Carbon* **2001**, *39*, 937.

(47) Hughes, M.; Shaffer, M. S. P.; Renouf, A. C.; Singh, C.; Chen, G. Z.; Fray, J.; Windle, A. H. *Adv. Mater.* **2002**, *14*, 382.

JP8049558